PAPER

Arrested coalescence in Pickering emulsions†

Amar B. Pawar,[ab] **Marco Caggioni,**[a] **Roja Ergun,**[b] **Richard W. Hartel**[b] **and Patrick T. Spicer**[*a]

When two emulsion drops begin to coalesce, their complete fusion into a single spherical drop can sometimes be arrested in an intermediate shape if a rheological resistance offsets the Laplace pressure driving force. Arrested coalescence of droplets is important, both for its broad impact on commercial food production as well as its potential for fabricating novel anisotropic colloidal microstructures. We use a micromanipulation technique to demonstrate the dynamics of arrested coalescence between droplets with interfacially adsorbed colloids. Surface coverage of the droplets is precisely determined by a capillary aspiration technique and then their coalescence is studied *in situ*. Depending on their surface coverage, droplets can experience total coalescence, arrested coalescence or total stability. We use microscopic observations along with geometrical packing arguments to confirm that coalescence is arrested due to close-packed jamming of particles. The anisotropic Laplace stress within the arrested structure is balanced by the elastic modulus of the jammed interface and thus further relaxation of the arrested structure is halted. Precise mapping of the arrested coalescence regime at a microscopic scale helps us to anticipate its effects on bulk scale production of such anisotropic colloidal structures.

1 Introduction

Numerous consumer products including foods, pharmaceuticals, shampoos and cosmetics contain emulsions: dispersions of two immiscible fluids.[1] Emulsions are thermodynamically unstable droplet dispersions that undergo coarsening by coalescence, a mechanism of film rupturing between adjacent droplets, which allows the recombination of individual droplets until two liquid phases completely separate out.[1,2] Stabilization against coalescence is normally achieved by additives that adsorb to the liquid–liquid interface and provide steric, electrostatic, or rheological resistance against droplet collision or recombination.[1] While surfactants are a common emulsion stabilizer, colloids are also useful when adsorbed at the liquid–liquid interface. These so-called Pickering emulsions[3] are reported to be stable against coalescence for a wide range of droplet surface coverage[4–9] and require particles that are partially wetted by both liquids, facilitating their adsorption at the interface.[10] While most studies consider spherical colloids; ellipsoids,[11] disc-shaped particles,[12] and irregularly-shaped aggregates of particles[13] also efficiently stabilize emulsions.

Between the extremes of total coalescence and the total stabilization of emulsions is a fascinating intermediate phenomenon: arrested coalescence. When two droplets collide and begin to coalesce, their further progress can be halted by opposing forces. The resultant arrested structure resembles a stable doublet that is a snapshot of an intermediate state of the coalescence process. The field of food science has extensively studied such coalescence behavior in dairy systems using the term "partial coalescence".[14] Essential for arrested coalescence to occur are conditions that allow droplets to initiate coalescence and a resistance that then halts it before completion, stabilizing the arrested structure against further shape relaxation. In commercial systems coalescence is generally initiated by shear[15,16] and is arrested by the resistance from interactions of solid fat crystals in foods[17] or wax crystals in non-food emulsions.[18] Various forms of arrested coalescence are seen in foods,[17,19–21] but the process is analogous to colloidal gelation as it yields a structure of interconnected droplets with a coordination number on the order of 3–5.[22,23] Although total coalescence can be undesirable in many emulsions, arrested coalescence is essential to the formation of desired microstructure in food products, such as ice cream and whipped cream.[16,24,25] Despite its broad occurrence in foods,[14,17,19–21,26,27] arrested coalescence is still not completely understood at a fundamental level. This is partly because arrested coalescence can occur as a result of different types of droplet–colloid interactions, including droplet bridging by colloids, either by coating[21] or when entirely contained within the droplets:[27] two radically different wetting states commonly found in complex food mixtures.

Though arrested coalescence is most often studied in commercial applications, recently simulations and studies of model systems have provided more fundamental insights.[28]

[a]*Complex Fluid Microstructures, Corporate Engineering, Procter and Gamble Co., 8256 Union Center Blvd., West Chester, Ohio, USA. E-mail: spicer.pt@pg.com*
[b]*University of Wisconsin, Department of Food Science, 105 Babcock Hall, 1605 Linden Drive, Madison, WI, USA*
† Electronic supplementary information (ESI) available: Movies S1–S4. See DOI: 10.1039/c1sm05457k

Jamming of polystyrene and silica colloids at the interface of bubbles[28–30] and water droplets[31] in microfluidics can form "armored" structures that preserve an irregular doublet as well as other shapes. Fascinating structures are also produced by arresting the interface of coarsening binary liquid mixtures by the jamming of interfacially adsorbed colloids, creating a bicontinuous jammed emulsion or "bijel".[32,33] Although a similar jamming of particles is operative during the arrested coalescence in food, bijels are truly bicontinuous whereas foods exhibit gelation with distinct droplet regions present.

While arrested coalescence has successfully created a range of bulk and particulate materials, even commercially available foods, direct observations of arrested coalescence have not been made. Most studies utilize bulk measures like rheology[34,35] or microscopic observations of already arrested structures[14,36] to infer the dynamics, but the small size and short time scales have, until now, prevented direct study of the initiation, arrest, and stabilization of coalescing drops. Although Cheng and Velankar[37] reported the arrest of single droplets by particle jamming in a spinning drop, the arrested coalescence of two drops has not been directly studied. Here, we use a micromanipulation technique to perform *in situ* observations of arrested coalescence between oil droplets with varying amounts of interfacially adsorbed silica colloids. Our technique enables us to determine the droplet surface coverage by colloids and to measure the droplet interfacial and mechanical properties to understand the criteria for arrested coalescence. We generalize our observations to form a conceptual model of Pickering droplet coalescence. Furthermore, we develop a structural map which delineates the surface coverage limits bounding total coalescence, total stability, and arrested coalescence. A physical model is put forward for the surface coverage criteria and the forces required to arrest coalescence. Using these concepts, we are able to comment on the significance of this type of arrested coalescence in commercial systems and better map the behavior of more idealized structures like bijels and armored drops.

2 Experimental details

First, oil-in-water (O/W) Pickering emulsions are fabricated and a diluted drop of the emulsion is used for capillary experiments. Surface coverage of the individual Pickering droplets is estimated by capillary aspiration experiments. Coalescence between two Pickering droplets is then monitored by their micromanipulation using two separate micropipettes.

2.1 Emulsion preparation

Prior to fabricating the emulsions, 3 wt% silica particles ($d = 1.5$ μm) are dispersed in hexadecane by sonication. Pickering emulsions are prepared by mixing equal volumes (5 ml each) of the colloid-hexadecane dispersion and DI-water for a minute in a mixer at ~4000 rpm (IKA Ultra-Turrax Turbo drive). The three-phase contact angle of the silica particles adsorbed at the O/W interface is measured by the gel-trapping technique[38] and is ~70°, measured from the water side. Hydrophilic silica particles preferentially adsorb at the droplet interface and stabilize the O/W emulsions.[10] The emulsions contain Pickering droplets of variable size (50–200 μm) and surface coverage (30–90%). For

capillary aspiration experiments, emulsions are further diluted (100 times) with a 0.5 wt% microfibrous cellulose (MFC, CP-Kelco, $\tau_y \sim 0.17$ Pa) dispersion. The MFC dispersion is used to arrest the uncontrolled motion of the Pickering droplets during micromanipulation experiments. A comparison with the coalescence behavior in a continuous phase without MFC indicates that the small yield stress does not appreciably change our results.

2.2 The capillary aspiration technique

A capillary aspiration technique[39] is used to estimate the surface coverage of the droplets by silica particles and to study the dynamics of their coalescence. The experimental set-up consists of a micropipette that is connected to a water reservoir (10 ml open syringe) by rubber tubing. Tapered micropipettes are fashioned from standard borosilicate glass capillaries (1 mm OD and 0.5 mm ID, Sutter Instruments) with a Micropipette Puller (Model P-97; Sutter Instruments). The tips of the micropipettes are flattened using a Microforge (Model MF-830; Narishige Int'l USA). A micropipette is mounted on a 3-axis coarse manipulator (Narishige Int'l USA), which is attached to a microscope stage (Zeiss axioplan-2). The hydrostatic pressure, applied using a micropipette, can be adjusted by controlling the height of a water reservoir connected to it. A diluted drop of the emulsion is placed on a glass slide and the micromanipulator is used to align the tip of the micropipette with respect to an emulsion droplet. The droplet is drawn toward the micropipette tip by applying suction (negative hydrostatic pressure) and, once captured, oil starts to squeeze out of the droplet inside the micropipette. The amount of oil squeezed out of the droplet is estimated by tracking the oil/water boundary inside the micropipette and is used to determine the droplet surface coverage by particles. The micromanipulation set-up is modified to accommodate another micropipette mounted on a separate manipulator. The dynamics of coalescence between two droplets are examined by contacting them while they are held at the tips of the two coaxially-aligned micropipettes.

3 Results and discussions

During the coalescence of two drops, interfacial tension drives coarsening of the resultant droplet toward a spherical shape. Coalescence reduces the interfacial area and, thus, is an energetically favorable transition. Fig. 1 illustrates the coalescence of two hexadecane drops without adsorbed colloids and plots the change in the total interfacial area with time. The somewhat slow time scale of coalescence seen here is the result of an increased continuous phase viscosity (200 cP at 10 s^{-1}) caused by the dispersed cellulose fibers. The interfacial area is reduced until it reaches the minimum, *i.e.*, the surface area of a totally coalesced spherical droplet (Fig. 1(f)). A reduction to 79% ($2^{-1/3}$) of the original interfacial area is achieved during the coalescence of two drops. Assuming rotational symmetry, the interfacial area is calculated by the numerical integration of the perimeters of the discs along the central axis of the coalescing shape. The coalescing microstructure progresses through various non-spherical profiles (Fig. 1(b)–(e)) before reaching the final spherical shape. These microstructures map an intermediate regime containing
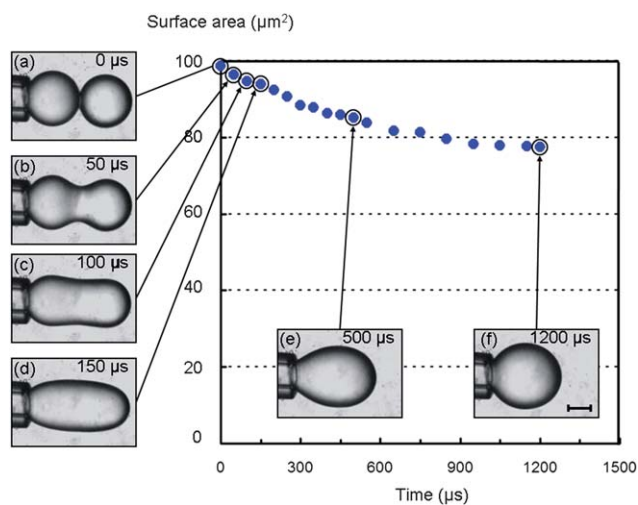
Fig. 1 Microphotographic montage of the coalescence dynamics between two hexadecane droplets and plot of the % change in the total surface area (100% being the total surface area of two droplets) against time as the coalescence proceeds. Images (b)–(e) represent intermediate microscopic images of coalescing droplets. The scale bar is 50 μm.

multiple, well-defined, short-lived shapes. The fabrication of stable forms of these anisotropic microstructures is practical if coalescence is arrested at any of these intermediate stages.

Compared to the bare droplets in Fig. 1, the adsorption of colloids at a droplet interface can add additional dynamics to the coalescence process. During the coalescence of Pickering droplets, particles can reorganize at the interface but their desorption is practically inhibited because of strong desorption energies, ∼7×10^6 kT for a 1.5 μm silica particle from the hexadecane/water interface ($\gamma = 42$ dyne cm^{-1})($E = \pi R_{particle}^2 \gamma (1 \pm \cos \theta)^2$).[10] While the interfacial area is being reduced, particles may get jammed at the interface, leading to a loss of interfacial mobility. Such a jammed interface exhibits solid-like characteristics[40–42] and can potentially arrest coalescence at the intermediate stages. For weak attractive interactions between particles, interfacial jamming occurs when particles become close-packed at the interface. Thus, surface coverage is a key parameter in arresting droplet coalescence.

3.1 Surface coverage determination by the capillary aspiration technique

The capillary aspiration technique enables us to precisely determine the surface coverage of individual droplets before studying their coalescence. A droplet is first captured at the tip of a micropipette. Once captured, suction pressure creates and stabilizes an oil/water interface inside the micropipette (Fig. 2 (a)). The magnitude of suction needed to stabilize the hemispherical interface can be obtained by a pressure balance equation:[43]

$$\Delta P_{suction} = 2\gamma \left(\frac{1}{R_{droplet}} - \frac{1}{R_{micropipette}} \right) \quad (1)$$

where $R_{droplet}$ and $R_{micropipette}$ are the droplet and the micropipette radii, respectively. If suction pressure is further increased, oil starts to flow out of the droplet inside the micropipette while
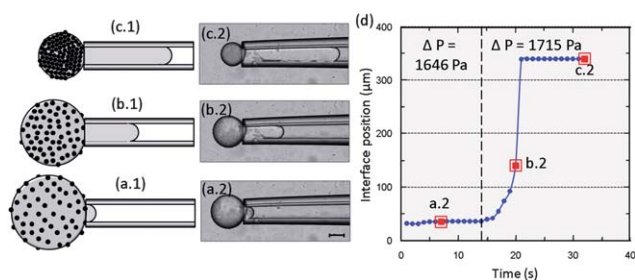
Fig. 2 The capillary aspiration experiment for determining the surface coverage of droplets by particles, (a.1–c.1) are schematic and (a.2–c.2) are the experimental images. (a) Suction pressure (1646 Pa) equilibrates the hemispherical O/W interface inside the micropipette. As the suction is increased (1715 Pa), oil is squeezed out of the droplet and into the pipette. (b) Intermediate position of the O/W interface inside the micropipette. (c) Equilibrated position of the O/W interface. Oil flow ceases due to particle jamming on the droplet interface. (d) Plot of the interface position inside the micropipette as the suction is increased from 1646 Pa to 1715 Pa. The scale bar = 50 μm.

the adsorbed particles remain behind on the droplet interface (Fig. 2(b)). As the oil flow continues, the droplet interfacial area is reduced and the surface coverage is increased accordingly. When interfacial area becomes comparable to the close-packed area of adsorbed particles, particles jam and the oil flow ceases (Fig. 2(c)). If suction pressure is further increased, the interface buckles[44–47] and eventually the droplet is completely withdrawn inside the micropipette. The dynamics of the oil flow can be monitored by plotting the O/W interface position inside the micropipette against time (Fig. 2(d)). The points (a.2), (b.2), and (c.2) correspond to intermediate snapshots in Fig. 2. This suction-dominated oil flow is analogous to the coalescence-induced oil flow from the droplet.

Once the oil flow ceases, oil can be returned to the droplet by increasing the hydrostatic pressure. The droplet regains its initial size and surface coverage but the original arrangement of particles can not be regained and more dense aggregates of the particles are observed at the droplet interface. Such a hysteresis in particle rearrangement is believed to be due to the slow relaxation of the compression-induced particle microstructure.[42] Assuming that the droplet interface is close-packed with particles when the oil flow ceases, the original droplet surface coverage can be estimated as,

$$\phi_{droplet} = \frac{0.9 \left(\dfrac{\frac{4}{3}\pi R_{droplet}^3 - V}{\frac{4}{3}\pi} \right)^{\frac{2}{3}}}{R_{droplet}^2} \quad (2)$$

where the factor 0.9 corresponds to the close-packed density of particles on a 2D plane surface[5] and $R_{droplet}$ is the initial droplet radius. V is the volume of oil that has been squeezed out of the droplet when the oil flow ceases and is estimated as the volume of a frustum with a hemispherical cap on its end:

$$V = \frac{\pi L}{12}(d_1^2 + d_1 d_2 + d_2^2) + \frac{\pi}{12}d_2^3 \quad (3)$$

where d_1 and d_2 are the initial and the final diameters of the oil slug, and L is the length of the slug. Any deviation of the

micropipette tip from the approximated frustum shape provides an error in the estimated surface coverage and so the volume, V, is additionally verified by measuring the difference in the volume of the droplet before and after squeezing out the oil. A 2% variability is observed in the estimated surface coverage when the volume, V, is measured by either of the techniques. Furthermore a small error is anticipated in the estimated surface coverage because the particles adsorbed on the O/W interface inside the micropipette are neglected in calculations.

3.2 Droplet coalescence behavior

Once the surface coverage of two drops is determined, the same drops can then be brought together manually to study their coalescence. As the partially covered Pickering droplets come into contact with one another, particles in the contact region are displaced away towards the periphery, forming a dense aggregated region surrounding the central contact area (Fig. 3(a)). Two vertically contacted droplets enable us to visualize the dimple formation in the contact region (Fig. 3(a)). Formation of such a dimple surrounded by a ring of particles has been reported earlier, when a partially covered droplet came into contact with a plane liquid interface.[48–50] The force required to push the particles inside the droplet is much higher than the force required to displace them laterally at the droplet interface.[4] And so, when the droplets touch, they form a dimple in the contact region (Fig. 3(b.1)) rather than forming a particle bridge[51] between them. If the droplets are further forced toward each other, the central dimple gradually flattens and eventually ruptures, initiating coalescence (Fig. 3(b.2)).

Fig. 4 demonstrates such a coalescence for two partially covered Pickering droplets. First a dimple forms in the contact area (Fig. 4(b)). The dimple then flattens and liquid oil begins to be exchanged between the droplets (Fig. 4(c)) as the coalescence is initiated. The viscous response of the interface allows the rearrangement of adsorbed particles. The Laplace pressure
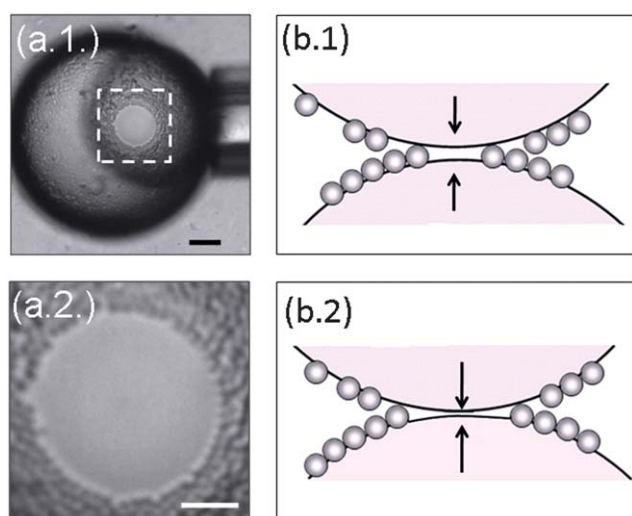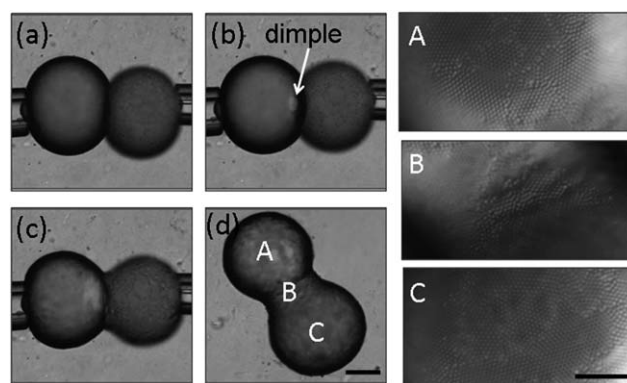
Fig. 4 Coalescence between two hexadecane droplets partially covered with silica particles. (a) Two droplets held at two micropipette tips are manually brought together for coalescence, (b) The dimple formation in the contact region, (c) Initiation of droplet coalescence, (d) Partially coalesced droplets maintaining their stability in the suspension. The scale bar is 50 μm. A, B, and C are detailed images of the close-packed particles on the partially coalesced droplet's interface and neck. The scale bar is 20 μm.

gradient governs the dynamics of fluid exchange and particle rearrangement. As the coalescence progresses, the interfacial area is gradually reduced and the surface coverage is increased accordingly. If sufficient particles are present (e.g., Fig. 4), coalescence continues until the fluid-like interface transitions to a rigid film of solid particles. In such an interface, the jammed particles arrest coalescence because the particles form a cohesive structure that resists the Laplace pressure gradient that drives the drops together. Additional shape relaxation of the arrested structure (Fig. 4(d)) is hindered as it requires further reduction in the interfacial area, either by the desorption of the particles from the interface or by the failure of the interfacial particle structure. Although the desorption energies of particles provide a sufficient barrier against their stochastic removal from the interface, some desorption of a few particles is observed at the instance of coalescence, likely due to flow instabilities during the rapid relaxation. Fig. 4(A)–(C) illustrate that the particle microstructure at the drop and neck interface is a close-packed arrangement that resists coalescence and stabilizes a non-spherical shape that is identical to Fig. 1(b).

The particle surface coverage of the droplets is a critical parameter that determines the timing of the arrest and thus, the shape of the arrested structure. Fig. 5 reports different microstructures obtained due to the coalescence of two Pickering droplets as a function of the initial surface coverage. Coalescence behavior can be divided into total stability (Fig. 5(a)), arrested coalescence (Fig. 5(b) and (c)), and total coalescence (Fig. 5(d)). If droplets are completely covered with particles (ϕ_1 and $\phi_2 \sim 0.9$), then they can not even initiate coalescence (Fig. 5(a)). For experimental observation of the total stability of the Pickering droplets, liquid oil is squeezed out of two droplets until the particles are jammed at their interface (condition for ϕ_1 and $\phi_2 \sim 0.9$) and then their coalescence is studied. Because the lateral movement of silica particles at the interface is halted, formation of a dimple in the contact region is avoided and stability against coalescence is achieved. This non-coalescing behavior of droplets explains the stability of Pickering emulsions

Fig. 3 (a.1) and (a.2): The dimple formation as two partially covered Pickering droplets touch. The scale bar for (a.1) = 25 μm and for (a.2) = 10 μm. (b.1) and (b.2) are the schematics of the dimple formation and coalescence initiation as the droplets are further forced toward each other.
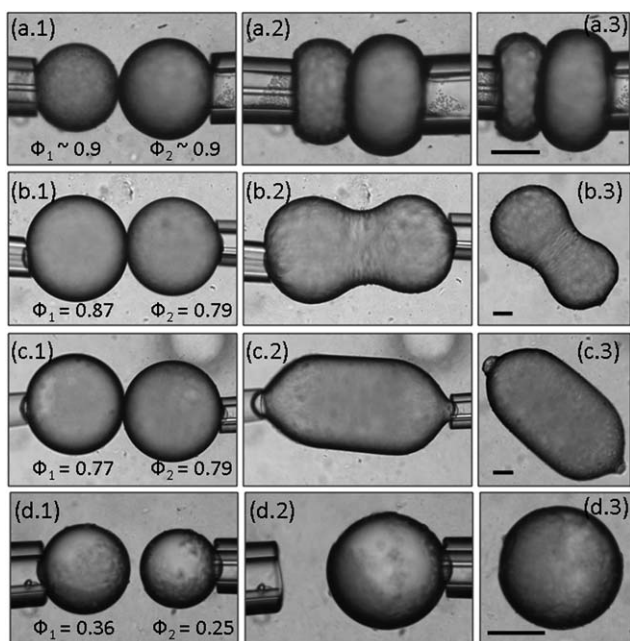
Fig. 5 Coalescence behavior as a function of the droplet surface coverage. (a) Total stability, (b) and (c) arrested coalescence, and (d) total coalescence of Pickering droplets. Scale bars = 50 μm. Please refer to the ESI† for coalescence movies.

Fig. 6 Different coalescence regimes (total coalescence, arrested coalescence and total stability) as a function of the droplet surface coverage. The dashed line indicates the surface coverage condition ($\phi_1 + \phi_2 = 1.43$). The dotted lines indicate the maximum surface coverage that the droplets can possess. Since ϕ_1 and ϕ_2 are interchangeable, the data is symmetrical.

by steric repulsion between completely covered droplets.[4,6,8–10] However, if the amount of particles is too sparse then total coalescence can occur (Fig. 5(d)). Within an intermediate surface coverage regime, arrested coalescence is observed (Fig. 5(b) and (c)) where the transition shapes observed during total coalescence (Fig. 1(b) and (d)) are now stabilized.

As the coalescence between the droplets is systematically examined for the variable surface coverage, a range of ϕ_1 and ϕ_2 is identified where various coalescence behaviors are exhibited. Fig. 6 indicates that total coalescence is dominant for most initial surface coverage values. At a higher surface coverage, there exists a narrow regime where arrested coalescence is favored. Depending on when coalescence is arrested, different shapes can be produced (Fig. 5(b) and (c)). Total stability against coalescence is observed only when the droplets are completely covered with particles. For these studies, since ϕ_1 and ϕ_2 are interchangeable, the data in Fig. 6 is symmetrical. The experimental data is obtained from the coalescence observations of droplets with similar sizes (5% size distribution).

Since the close-packed ($\phi = 0.9$) interfacial jamming of particles arrests coalescence, it sets bounds on the surface coverage (ϕ_1 and ϕ_2) where the arrested coalescence of two droplets is expected. If the combined surface area occupied by particles is higher than the interfacial area expected to form by the total coalescence of two droplets, then coalescence is arrested. The surface coverage condition for arrested coalescence is given as:

$$\left[0.9 \times 4\pi\left(R_1^3 + R_2^3\right)^{\frac{2}{3}}\right] < (\phi_1 A_1 + \phi_2 A_2) < 1.81 \qquad (4)$$

where ($\phi_1 A_1 + \phi_2 A_2$) is the combined surface area occupied by the particles on two individual drops. The lower bound on the surface area represents the surface area available for particles as

a result of total coalescence between two droplets (radii R_1 and R_2). A_1 and A_2 are the interfacial areas of droplets with radii R_1 and R_2 ($A_1 = 4\pi R_1^2$). The upper bound dictates the maximum combined surface coverage of two drops and is the condition for the total stability of Pickering droplets. For arresting coalescence of identical droplets ($R_1 = R_2$), eqn (4) can be simplified as:

$$1.43 < (\phi_1 + \phi_2) < 1.81 \qquad (5)$$

The surface coverage condition ($\phi_1 + \phi_2 = 1.43$) marks the boundary between total coalescence and arrested coalescence and is plotted by a dashed line in Fig. 6. Any excess particles (higher surface coverage) arrest coalescence before reaching a spherical shape and any deficiency of particles (lower surface coverage) results in a totally coalesced spherical droplet. The observed experimental coalescence behavior is in excellent agreement with geometrical packing theory predictions for monodisperse spheres (eqn (5)). In a few cases, arrested coalescence occurs slightly below the ($\phi_1 + \phi_2 = 1.43$) line but this small deviation most likely reflects the error in approximating close packing on a spherical surface by the value for a plane surface. Similar coalescence regimes are expected for polydisperse colloids, but variations in the packing efficiency may shift the transitions between the regimes to different surface coverage conditions than for monodisperse colloids (eqn (5)). Microscopic observations of close-packed particles on the interface (Fig. 4 (A)–(C)) along with the excellent agreement between experimental and predicted data (Fig. 6) confirms that any particle rearrangement hysteresis during capillary aspiration does not significantly affect our results.

Arrested non-spherical doublet microstructures possess definite internal stress due to the Laplace pressure imbalance:

$$\Delta P = \frac{2\gamma}{R_{\text{droplet}}} - \left(\frac{\gamma}{R_1} - \frac{\gamma}{R_2}\right) \qquad (6)$$

Fig. 7 Partially coalesced doublet of Pickering droplets observed in emulsion prepared using bulk mixing.

where R_1 (cross-sectional radius) and R_2 (neck radius) are the two principal radii characterizing the curvature of the neck.[52,53] The partially coalesced droplets indicated in Fig. 5(b.3) and (c.3) possess a Laplace pressure gradient of $\Delta P = 6.81 \times 10^2$ Pa ($R_{droplet} = 100$ μm, $R_1 = 48$ μm, and $R_2 = 73$ μm) and $\Delta P = 5.63 \times 10^2$ Pa ($R_{droplet} = 94$ μm, $R_1 = 94$ μm, and $R_2 = \inf$) respectively. In order for arrested structures to be stable, the Laplace pressure imbalance must be offset by the elasticity of the jammed interface. The Young's modulus of the interface covered with close-packed particles ($\theta = 90°$) can be estimated as:[44]

$$E_{close\text{-}pack} = 4.54 \frac{\gamma}{D_{particle}} \qquad (7)$$

The solid-like interface will deform in response to the Laplace stress. Due to a higher magnitude of the elastic modulus (128×10^3 Pa), the corresponding strain is negligible (<1%) and thus, further deformation of the arrested structures' interface is avoided.[36] There may be coupling between the yield stresses of the interface and the continuous phase[54] and, while such interaction can affect the interfacial contributions to arrested coalescence, we observed similar arrests in water without MFC present and feel that our results are not significantly affected.

4 Conclusions

Direct observation and characterization of the arrested coalescence of Pickering droplets is performed. We map and determine the surface fraction criteria for total coalescence, arrested coalescence, and the total stability of the Pickering droplets. During coalescence, the interfacial area is gradually reduced, leading to an increased surface coverage. As the interfacial area equals the area needed for close-packing of particles, the particles jam at the interface and freeze the non-spherical shape at an intermediate stage of coalescence without any further shape relaxation: arrested coalescence. Arrested coalescence requires a surface coverage that permits the initiation of coalescence but arrests it before its completion into a spherical droplet. Jammed particles impart a solid-like interface to the drops that sustain the anisotropic stresses existing in the arrested microstructure. We propose packing arguments that accurately describe the experimentally observed coalescence behaviors and provide the limiting bounds of surface coverage where arrested coalescence is expected. Formation of such non-spherical droplets by arrested coalescence is rare (Fig. 7) when Pickering emulsions are made *via* bulk mixing, because the phenomena require the initiation of coalescence between droplets with reasonably precise surface

coverage. But instead, it appears that the droplets grow in size by total coalescence until complete surface coverage is achieved.[8]

Once the coalescence of the two Pickering droplets is arrested, the entire interface is covered with jammed particles. Identical to the conventional steric stabilization of Pickering emulsions, coalescence of any additional droplet with the arrested structure is impossible, inhibiting the formation of drop networks. However, ternary and other multiunit structures have been reported earlier.[31] These higher order structures are the result of local interfacial jamming of particles, like in the coalescing neck region, rather than on the entire droplet interface. One explanation for these differences is that the surfactant in these emulsions can significantly modify the particle interactions on Pickering droplets and a very different droplet coalescence behavior can be observed. For example, more attractive particles can jam at a much lower surface coverage than 0.9 and significantly broaden the regime of arrested coalescence. Here, we limited our study to a single set of interfacial conditions but will later examine additional cases, including modified particle interactions.

References

1 B. P. Binks, *Modern Aspects of Emulsion Science*, The Royal Society of Chemistry, 1998.
2 D. J. McClements, *Food Emulsions: Principles, Practices, and Techniques*, CRC Press, 2005.
3 S. U. Pickering, *J. Chem. Soc.*, 1907, **91**, 2001–2021.
4 D. E. Tambe and M. M. Sharma, *Adv. Colloid Interface Sci.*, 1994, **52**, 1–63.
5 S. Reynaert, P. Moldenaers and J. Vermant, *Phys. Chem. Chem. Phys.*, 2007, **9**, 6463–6475.
6 B. R. Midmore, *Colloids Surf., A*, 1998, **132**, 257–265.
7 E. Vignati, R. Piazza and T. P. Lockhart, *Langmuir*, 2003, **19**, 6650–6656.
8 S. Arditty, C. P. Whitby, B. P. Binks, V. Schmitt and F. Leal-Calderon, *Eur. Phys. J. E*, 2003, **11**, 273–281.
9 C. Zeng, H. Bissig and A. D. Dinsmore, *Solid State Commun.*, 2006, **139**, 547–556.
10 B. P. Binks, *Curr. Opin. Colloid Interface Sci.*, 2002, **7**, 21–41.
11 S. Vandebril, J. Vermant and P. Moldenaers, *Soft Matter*, 2010, **6**, 3353–3362.
12 N. P. Ashby and B. P. Binks, *Phys. Chem. Chem. Phys.*, 2000, **2**, 5640–5646.
13 B. P. Binks, P. D. Fletcher, B. L. Holt, J. Parker, P. Beaussoubre and K. Wong, *Phys. Chem. Chem. Phys.*, 2010, **12**, 11967–11974.
14 K. Boode, P. Walstra and A. E. A. de Groot-Mostert, *Colloids Surf., A*, 1993, **81**, 139–151.
15 F. Thivilliers-Arvis, E. Laurichesse, V. Schmitt and F. Leal-Calderon, *Langmuir*, 2010, **26**, 16782–16790.
16 H. D. Goff, *J. Dairy Sci.*, 1997, **80**, 2620–2630.
17 P. Walstra, *Physical Chemistry of Foods*, Marcel Dekker Inc., 2003.
18 J. Giermanska, F. Thivilliers, R. Backov, V. Schmitt, N. Drelon and F. Leal-Calderon, *Langmuir*, 2007, **23**, 4792–4799.
19 K. Boode and P. Walstra, *Colloids Surf., A*, 1993, **81**, 121–137.
20 D. Johansson, B. Bergenstahl and E. Lundgren, *J. Am. Oil Chem. Soc.*, 1995, **72**, 939–950.
21 E. Dickinson, *Curr. Opin. Colloid Interface Sci.*, 2010, **15**, 40–49.
22 E. Zaccarelli, *J. Phys.: Condens. Matter*, 2007, **19**, 323101.

23 J. Brujic, C. Song, P. Wang, C. Briscoe, G. Marty and H. A. Makse, *Phys. Rev. Lett.*, 2007, **98**, 248001.

24 J. Benjamins, M. H. Vingerhoeds, F. D. Zoet, E. de Hoog and G. A. van Aken, *Food Hydrocolloids*, 2009, **23**, 102–115.

25 D. Rousseau, *Food Res. Int.*, 2000, **33**, 3–14.

26 V. M. Boekel and P. Walstra, *Colloids Surf.*, 1981, **3**, 109–118.

27 E. Fredrick, P. Walstra and K. Dewettinck, *Adv. Colloid Interface Sci.*, 2010, **153**, 30–42.

28 A. B. Subramaniam, M. Abkarian, L. Mahadevan and H. A. Stone, *Langmuir*, 2006, **22**, 10204–10208.

29 A. B. Subramaniam, M. Abkarian, L. Mahadevan and H. A. Stone, *Nature*, 2005, **438**, 930–930.

30 A. B. Subramaniam, M. Abkarian and H. A. Stone, *Nat. Mater.*, 2005, **4**, 553–556.

31 A. R. Studart, H. C. Shum and D. A. Weitz, *J. Phys. Chem. B*, 2009, **113**, 3914–3919.

32 K. Stratford, R. Adhikari, I. Pagonabarraga, J.-C. Desplat and M. E. Cates, *Science*, 2005, **309**, 2198–2201.

33 E. M. Herzig, K. A. White, A. B. Schofield, W. C. K. Poon and P. S. Clegg, *Nat. Mater.*, 2007, **6**, 966–971.

34 F. Thivilliers, E. Laurichesse, H. Saadaoui, F. Leal-Calderon and V. Schmitt, *Langmuir*, 2008, **24**, 13364–13375.

35 F. Thivilliers, N. Drelon, V. Schmitt and F. Leal-Calderon, *Europhys. Lett.*, 2006, **76**, 332–338.

36 P. S. Clegg, E. M. Herzig, A. B. Schofield, T. S. Horozov, B. P. Binks, M. E. Cates and W. C. K. Poon, *J. Phys.: Condens. Matter*, 2005, **17**, S3433–S3438.

37 H. L. Cheng and S. S. Velankar, *Langmuir*, 2009, **25**, 4412–4420.

38 V. N. Paunov, *Langmuir*, 2003, **19**, 7970–7976.

39 S. Lee, D. H. Kim and D. Needham, *Langmuir*, 2001, **14**, 5537–5543.

40 B. Madivala, S. Vandebril, J. Fransaer and J. Vermant, *Soft Matter*, 2009, **5**, 1717–1727.

41 H. Xu, S. Melle, K. Golemanov and G. Fuller, *Langmuir*, 2005, **21**, 10016–10020.

42 C. Monteux, J. Kirkwood, H. Xu, E. Jung and G. G. Fuller, *Phys. Chem. Chem. Phys.*, 2007, **9**, 6344–6350.

43 R. Kwok and E. Evans, *Biophys. J.*, 1981, **35**, 637–652.

44 D. Vella, P. Aussillous and L. Mahadevan, *Europhys. Lett.*, 2004, **68**, 212–218.

45 B. P. Binks and T. S. Horozov, *Colloidal particles at liquid interfaces*, Cambridge University Press, 2006.

46 S. S. Datta, H. C. Shum and D. A. Weitz, *Langmuir*, 2010, **26**, 18612–18616.

47 S. O. Asekomhe, R. Chiang, J. H. Masliyah and J. A. W. Elliott, *Ind. Eng. Chem. Res.*, 2005, **44**, 1241–1249.

48 E. J. Stancik, M. Kouhkan and G. G. Fuller, *Langmuir*, 2004, **20**, 90–94.

49 T. S. Horozov, *Curr. Opin. Colloid Interface Sci.*, 2008, **13**, 134–140.

50 K. P. Velikov, F. Durst and O. D. Velev, *Langmuir*, 1998, **14**, 1148–1155.

51 T. S. Horozov and B. P. Binks, *Angew. Chem. Int. Ed.*, 2006, **45**, 773–776.

52 H. J. Butt, K. Graf and M. Kappl, *Physics and Chemistry of Interfaces*, Wiley VCH GmbH and Co. KGaA, 2003.

53 J. N. Israelachvili, *Intermolecular and Surface Forces*, Academic Press, 1997.

54 P. Thareja and S. Velankar, *Rheol. Acta*, 2007, **46**, 405–412.